Supplement to "Below-cloud scavenging of aerosol by rain: A review of numerical modelling approaches" by A.C. Jones *et al.*

S1 Terminal velocity of falling droplets and particles

Reynold's number R_e, a measure of whether flow is laminar or turbulent around an obstacle, is dependent on the terminal velocity of the particulate being measured. This creates an issue for liquid particles with diameter (D_d) greater than 20 μm that do not remain spherical as they fall. For these larger particles (e.g., rain droplets) implicit formulae following Beard (1976) are used.

Firstly, we define fundamental variables which will be used throughout this Supplement. Equation S1 is the ideal gas law which relates air density (ρ_a, kg m^{-3}) to air pressure (P_a, Pa), temperature (T_a, K), and the specific gas constant ($R_a = 287.05$ J kg^{-1} K^{-1}). Equation S2 relates the mean speed of air molecules (v_a, m s^{-1}) to the Boltzmann constant ($k_B = 1.3804 \times 10^{-23}$J K^{-1}), T_a, and the molecular mass ($m_a = 4.78 \times 10^{-26}$ kg). Equation S3 is the Sutherland Law according to List (1984), which relates the dynamic viscosity of air (μ_a, kg m^{-1} s^{-1}) to T_a. The constants in Eq. S3 are $S = 120$ K, $T_0 = 296.16$ K, and $\mu_0 = 1.83 \times 10^{-5}$ kg m^{-1} s^{-1}. Equation S4 relates the mean free path of air molecules (λ_a, m) to μ_a, ρ_a, and v_a. These variables are already used throughout UKCA-mode. μ_a and λ_a are determined at the start of the timestep in UKCA-mode.

$$\rho_a = \frac{P_a}{R_a T_a} \quad \text{(Eq. } S1\text{)}$$

$$v_a = \left(\frac{8k_B T_a}{\pi m_a}\right)^{1/2} \quad \text{(Eq. } S2\text{)}$$

$$\mu_a = \mu_0 \left(\frac{T_0 + S}{T_a + S}\right)\left(\frac{T_a}{T_0}\right)^{3/2} \quad \text{(Eq. } S3\text{)}$$

$$\lambda_a = \frac{2\mu_a}{\rho_a v_a} \quad \text{(Eq. } S4\text{)}$$

Next, we determine the terminal velocity of rain droplets ($U_t(D_d)$, m s^{-1}) according to Beard (1976) for 3 regimes: small cloud droplets ($0.5\mu m < D_d < 19\mu m$), large cloud droplets or small rain droplets ($19\mu m < D_d < 1.07mm$), and rain droplets ($1.07mm < D_d < 7mm$).

For $0.5\mu m < D_d < 19\mu m$, the terminal velocity is given from the product of the Stoke's velocity for a rigid sphere and the slip correction or Cunningham factor (Eqs S5-S6).

$$U_t(D_d) = \frac{{D_d}^2(\rho_w - \rho_a)g}{18\mu_a} \times C_c(D_d) \quad \text{(Eq. } S5\text{)}$$

$$C_c(D_d) = 1 + \frac{2\lambda_a}{D_d}\left(1.257 + 0.4\exp\left(-\frac{1.1D_d}{2\lambda_a}\right)\right) \quad \text{(Eq. } S6\text{)}$$

In Eq. S5, ρ_w is the density of water $\rho_w = 997$ kg m^{-3} while g is the gravitational acceleration constant ($g = 9.8$ m s^{-2}).

For $19\mu\text{m} < D_d < 1.07\text{mm}$, one needs to use the drag coefficient C_D as an empirical means to represent the drag force on the droplet (Seinfeld and Pandis, 1998). Unfortunately, C_D is a function of the Reynold's number ($R_{e,D}$) and thus the terminal velocity U_t and we need to determine U_t implicitly. To do this, we form the dimensionless variable $C_D{R_{e,D}}^2$ (widely known as the Davies number, Eq. S7) which can then be used to determine $R_{e,D}$, which is finally used to determine $U_t(D_d)$. The algorithm according to Beard (1976) is given below.

$$X = \ln\left(C_D{R_e}^2\right) = \ln\left(\frac{4{D_d}^3\rho_a(\rho_w - \rho_a)g}{3{\mu_a}^2}\right) \quad \text{(Eq. } S7\text{)}$$

$$Y = \sum_{i=0}^{6} a_i X^i \quad \text{(Eq. } S8\text{)}$$

$$R_{e,D} = C_c(D_d) \times \exp(Y) \quad \text{(Eq. } S9\text{)}$$

$$U_t(D_d) = \frac{\mu_a R_{e,D}}{\rho_a D_d} \quad \text{(Eq. } S10\text{)}$$

The coefficients in Eq. S8 are: $a_0 = -0.318657 \times 10^1$, $a_1 = +0.992696 \times 10^0$, $a_2 = -0.153193 \times 10^{-2}$, $a_3 = -0.987059 \times 10^{-3}$, $a_4 = -0.578878 \times 10^{-3}$, $a_5 = +0.855176 \times 10^{-4}$, and $a_6 = -0.327815 \times 10^{-5}$.

A similar approach is required for rain droplets with diameters of $1.07\text{mm} < D_d < 7\text{mm}$. Firstly, it is necessary to construct a formula for the surface tension of the droplet ($\sigma_{w,a}$, N m^{-1}) as a function of temperature in order to calculate the dimensionless Bond number. The surface tension decreases as temperature decreases and be described empirically using formulae for $-40^\text{o}\text{C} < T_c < 0^\text{o}\text{C}$ from Pruppacher and Klett (2010) and $T_c > 0^\text{o}\text{C}$ from Bohren and Albrecht (1998).

For $-40^\text{o}\text{C} < T_c < 0^\text{o}\text{C}$:

$$\sigma_{w,a} = 0.001 \times \begin{pmatrix} 75.93 + 0.115\,T_c + 6.818 \times 10^{-2}\,{T_c}^2 + \\ 6.511 \times 10^{-3}\,{T_c}^3 + 2.933 \times 10^{-4}\,{T_c}^4 + \\ 6.283 \times 10^{-6}\,{T_c}^5 + 5.285 \times 10^{-8}\,{T_c}^6 \end{pmatrix} \quad \text{(Eq. } S11\text{)}$$

For $T_c > 0^\text{o}\text{C}$:

$$\sigma_{w,a} = 0.2358 \times \left(\frac{374 - T_c}{647.15}\right)^{1.256} \times \left[1 - 0.625 \times \left(\frac{374 - T_c}{647.15}\right)\right] \quad \text{(Eq. } S12\text{)}$$

It is inconvenient to have two separate formulae for one covariate. Rather, it makes more sense to fit a polynomial to the combined $\sigma_{w,a}$ distribution. We use the function polyfit in the python library numpy.polynomial.polynomial to fit a polynomial with 6 degrees of freedom to $\sigma_{w,a}$ for $-40^{\mathrm{o}}\mathrm{C} < T_c < 100^{\mathrm{o}}\mathrm{C}$, but in terms of the temperature in K where $T_a = T_c + 273.15$. The polynomial is then:

$$\begin{aligned}\sigma_{w,a} = {} & 5.1877565 \times 10^{1} - 1.01222192 \times 10^{0}\, {T_a}^{2} + 8.21706952 \times 10^{-3}\, {T_a}^{2} \\ & -3.54598144 \times 10^{-5}\, {T_a}^{3} + 8.57833352 \times 10^{-8}\, {T_a}^{4} \\ & -1.10306055 \times 10^{-10}\, {T_a}^{5} + 5.88999924 \times 10^{-14}\, {T_a}^{6}\end{aligned} \quad \text{(Eq. } S13\text{)}$$

Supplementary Figure S1 shows the surface tension as a function of temperature (in $^{\mathrm{o}}$C) for the combined empirical formulae (Eg. S11 and Eq. S12) and the polynomial fit (Eq. S13), along with a linear fit used in the Cloud–AeroSol Interacting Microphysics (CASIM) module (Hill *et al.*, 2015) in which $\sigma_{w,a} = (7.61 - 0.155\, T_c) \times 10^{-3}$. It is clear that the polynomial is sufficient for our purposes, even reconciling the inconsistency between Eqs S11 and S12 at $T_c = 0^{o}C$.

Having determined the surface tension, we use it to define two more dimensionless variables: The Bond number (B_o, a measure of the relative importance of gravitational forces to surface tension) and N_p or the ratio of the Davies number to the Bond number to remove the diameter dependency.

$$B_o = \frac{4{D_d}^{2}(\rho_w - \rho_a)g}{3\sigma_{w,a}} \quad \text{(Eq. } S14\text{)}$$

$$N_p = \frac{{\sigma_{w,a}}^{3}{\rho_a}^{2}}{{\mu_a}^{4}(\rho_p - \rho_a)g} \quad \text{(Eq. } S15\text{)}$$

The algorithm to determine $R_{e,D}$ and U_t proceeds as follows

$$X = \ln\left(B_o {N_p}^{1/6}\right) \quad \text{(Eq. } S16\text{)}$$

$$Y = \sum_{i=0}^{5} b_i X^i \quad \text{(Eq. } S17\text{)}$$

$$R_{e,D} = {N_p}^{1/6} \times \exp(Y) \quad \text{(Eq. } S18\text{)}$$

$$U_t(D_d) = \frac{\mu_a R_{e,D}}{\rho_a D_d} \quad \text{(Eq. } S19\text{)}$$

The coefficients in Eq. S17 are: $b_0 = -0.500015 \times 10^{1}$, $b_1 = +0.523778 \times 10^{1}$, $b_2 = -0.204914 \times 10^{1}$, $b_3 = +0.475294 \times 10^{0}$, $b_4 = -0.542819 \times 10^{-1}$, and $b_5 = +0.238449 \times 10^{-2}$.

In the single moment UKCA-mode impaction scavenging scheme, $U_t(D_d)$ is parameterised using a very simple formula dependent only on the rain droplet diameter D_d (Eq. S20).

$$U_t(D_d) = \begin{cases} 4055\, D_d & D_d < 10^{-3}\text{m} \\ 130\, D_d{}^{\frac{1}{2}} & D_d \geq 10^{-3}\text{m} \end{cases} \quad (\text{Eq. } S20)$$

While it may be pragmatic to use a simple parameterisation (rather than the complex Beard (1976) scheme above), it is clear from Supplementary Fig. S2 that the UKCA-mode scheme overestimates U_t by orders of magnitude when $D_d < \sim 10^{-4}$m and does not capture the exponential decay in U_t for $D_d > \sim 10^{-3}$m. Given the fact that the rain droplet diameters are prescribed in UKCA-mode, it may also be prudent to prescribe terminal velocities using, say P=800mb and T=15°C. If a parameterisation is needed, then it may be prudent to use a 6th order polynomial of D_d with D_d in units of mm, which broadly captures both the logarithmic and linear relation between U_t and D_d for $D_d < 7$mm.

$$U_t(D_d) = 10^{\Sigma_1^6 c_i (\log_{10} D_d)^i} \quad (\text{Eq. } S21)$$

Given D_d in units of mm, the coefficients in Eq. S21 are $c_0 = 0.63357089$, $c_1 = 0.82965738$, $c_2 = -0.37507553$, $c_3 = 0.01117498$, $c_4 = -0.05815324$, $c_5 = -0.04914836$, and $c_6 = -0.00844277$. Figure S2 shows that the fit does a very good job of capturing both the logarithmic and linear relationship. Adding a temperature and pressure dependence may over complicate the algorithm. Note though, that in the Python script used in the manuscript, the full Beard's scheme (with a temperature dependence) and not Eq. S21 is employed. The advantage of using Eq. S21 over Beard's approach or the UKCA-mode approach is that it is unconditional and thus saves computational expense.

Following the calculation of $U_t(D_d)$, Reynold's number R_e is redetermined using Eq. S22, which is actually the Reynold's number based on the raindrop radius rather than diameter (compare with Eq. S10).

$$R_{e,r} = \frac{U_t(D_d)\rho_a D_d}{2\mu_a} \quad (\text{Eq. } S22)$$

S2 Rain droplet size distribution

The rain droplet size distribution in expressed as the number density for droplet diameters between D_d and $D_d + \Delta D_d$, $N(D_d)$ in units of m^{-3} m^{-1}. $N(D_d)$ is typically expressed as a function of the rainfall rate R, which is typically given in units of kg m^{-2} s^{-1}, mm hr^{-1}, or mm day^{-1}. It is straightforward to convert between these units given that 1 kg m^{-2} s^{-1} equals 1 mm and only a temporal conversion is necessary. For this formulation R is given in units of mm hr^{-1} while D_d is expressed in m. The relationship between R and the rain droplet distribution is then:

$$R = 3600 \times \int_0^\infty \frac{\rho_w \pi}{6} {D_d}^3 N(D_d) U_t(D_d) dD_d \quad \text{(Eq. } S23\text{)}$$

$U_t(D_d)$ has been discussed in detail. In single moment droplet models, $N(D_d)$ is typically parameterised using a Gamma distribution with the following probability density function.

$$N(D_d) = N_0 {D_d}^\mu e^{-\lambda D_d} \quad \text{(Eq. } S24\text{)}$$

In Eq. S24, the parameters N_0, λ, and μ describe the intercept, slope, and shape of the Gamma distribution. N_0 has units of m^{-3} m^{-1} and λ has units of m^{-1}. In this work, we adopt the common assumption such that $\mu = 0$ which reduces the Gamma distribution to a simpler exponential distribution (Eq. S25).

$$N(D_d) = N_0 e^{-\lambda D_d} \quad \text{(Eq. } S25\text{)}$$

Empirical parameterisations have been made between the observed R and $N(D_d)$. The most widely utilised $N(D_d)$ parameterisation is from Marshall and Palmer (MP, 1948).

$$N_0 = 8 \times 10^6 \quad \text{(Eq. } S26\text{)}$$

$$\lambda = 4.1 \times 10^3 \, R^{-0.21} \quad \text{(Eq. } S27\text{)}$$

Another widely utilised parameterisation was provided by Sekhon and Srivastava (SS, 1971), which improves on MP by constraining the (positive) relationship between N_0 with R using observations.

$$N_0 = 7 \times 10^6 \, R^{0.37} \quad \text{(Eq. } S28\text{)}$$

$$\lambda = 3.8 \times 10^3 \, R^{-0.14} \quad \text{(Eq. } S29\text{)}$$

Finally, Abel and Boutle (AB, 2012) empirically fitted N_0 to λ using a power law. They also derived a relationship between λ and R by assuming $U_t(D_d) = c_R {D_d}^{d_R}$, where the constants $c_R = 386.6$ and $d_R = 0.67$ are from Sachidananda and Zrnic (1986). By inputting $N(D_d)$ (Eq. S25) and $U_t(D_d)$ into Eq. S23, and making use of the Gamma function, AB derived the following formulae for N_0 and λ :

$$\lambda = \left(\frac{\pi \rho_w x_1 c_R \Gamma(4 + d_R + \mu)}{6 \, R / 3600} \right)^{\frac{1}{4+d+\mu-x_2}} \approx 6.236 \times 10^3 \, R^{-0.4} \quad \text{(Eq. } S30\text{)}$$

$$N_0 = x_1 \lambda^{x_2} \approx 4.9 \times 10^7 \, R^{-0.89} \quad \text{(Eq. } S31\text{)}$$

AB derived $x_1 = 0.22$ and $x_2 = 2.2$ empirically from observations which completes the model. Note that $\mu = 0$ in Eq. S30 under the assumption of an exponential distribution, as used in the UM.

S3 The collision efficiency according to Slinn (1984)

The collision efficiency $E(D_d, d_p)$ is defined as the ratio of the total number of collisions occurring between droplets and particles to the total number of particles in an area equal to the droplet's effective cross-sectional area, where d_p is the diameter of the collected particles (Seinfeld and Pandis, 1998). It is used in the formulation of the scavenging coefficient $\Lambda(d_p)$ (Eqs S32-S33).

$$\frac{dn(d_p)}{dt} = -\Lambda(d_p)n(d_p) \quad \text{(Eq. } S32\text{)}$$

$$\Lambda(d_p) = \int_0^\infty \frac{\pi}{4} {D_d}^2 U_t(D_d) E(D_d, d_p) N(D_d) dD_d \quad \text{(Eq. } S33\text{)}$$

In Eq. S32, $n(d_p)$ is the number density of aerosol particles with diameter d_p and $\Lambda(d_p)$ is the size-resolved scavenging coefficient (s^{-1}). Equation S33 relates $\Lambda(d_p)$ to the integral of the collision efficiency $E(D_d, d_p)$ over the rain droplet size distribution. The next issue is to provide an explicit formulation of $E(D_d, d_p)$ in terms of readily attainable parameters. The collection efficiency is assumed to be a linear combination of various processes that result in the collection of particles by droplets. The classical Slinn (1984) model combines three such processes: Brownian diffusion, interception, and impaction.

The Slinn (1984) model makes use of 5 dimensionless parameters used to characterise the collected particle and the flow around the rain droplet. It is empirical in nature, being based on laboratory data. Following Seinfeld and Pandis (1998) and Wang *et al.* (2010) the dimensionless parameters are:

$$R_{e,r}(D_d) = \frac{U_t(D_d)\rho_a D_d}{2\mu_a} \quad \text{(Eq. } S34\text{)}$$

$$S_c(d_p) = \frac{\mu_a}{\rho_a D_{\text{diff}}(d_p)} \quad \text{(Eq. } S35\text{)}$$

$$S_t(D_d, d_p) = \frac{2\tau(d_p)\left(U_t(D_d) - u_t(d_p)\right)}{D_d} \quad \text{(Eq. } S36\text{)}$$

$$\phi(D_d, d_p) = \frac{d_p}{D_d} \quad \text{(Eq. } S37\text{)}$$

$$\omega = \frac{\mu_w}{\mu_a} \quad \text{(Eq. } S38\text{)}$$

Two approximations have been made in Eqs S34-S38. Firstly, that the terminal velocity of the raindrop far exceeds the terminal velocity of the particle ($U_t(D_d) \gg u_t(d_p)$), and secondly that the squared sum of the raindrop and particle diameters is effectively equal to the square of the raindrop diameter alone ($(D_d + d_p)^2 \cong {D_d}^2$). Thus, we effectively assume that the raindrop diameter is much greater than the

particle diameter. Equations S34-S38 describe the Reynolds number with respect to radius (Eq. S34); Schmidt number (Eq. S35); Stokes number (Eq. S36); ratio of diameters (Eq. S37); and the viscosity ratio of water to air (Eq. S38). The parameters are further detailed below. With these dimensionless variables defined, Slinn (1984) then provided empirically derived formulae for the combined collision efficiency (Eqs S39-S42).

$$E_{\text{slinn}}(D_d, d_p) = E_{br}(D_d, d_p) + E_{in}(D_d, d_p) + E_{im}(D_d, d_p) \quad \text{(Eq. } S39\text{)}$$

$$E_{br}(D_d, d_p) = \frac{4}{R_{e,r} S_c}\left[1 + 0.4 {R_{e,r}}^{\frac{1}{2}} {S_c}^{\frac{1}{3}} + 0.16 {R_{e,r}}^{\frac{1}{2}} {S_c}^{\frac{1}{2}}\right] \quad \text{(Eq. } S40\text{)}$$

$$E_{in}(D_d, d_p) = 4\phi\left[\omega^{-1} + \left(1 + 2{R_{e,r}}^{\frac{1}{2}}\right)\phi\right] \quad \text{(Eq. } S41\text{)}$$

$$E_{im}(D_d, d_p) = \begin{cases} \left(\dfrac{S_t - {S_t}^*}{S_t - {S_t}^* + {}^2/_3}\right)^{3/2} \left(\dfrac{\rho_w}{\rho_p}\right)^{1/2} \times & S_t > {S_t}^* \\ 10^{2.905 - 3.07\left(\log_{10}\frac{S_t}{{S_t}^*}\right)^{0.173} - 2.61\times10^{-14} {R_{e,D}}^{3.9}} & \\ 0 & S_t \le {S_t}^* \end{cases} \quad \text{(Eq. } S42\text{)}$$

The exponent in the second line in Eq. S42 is an empirical correction factor introduced by Fredericks and Saylor (2016). ρ_p is the particle density assumed to be 1500 kg m^{-3}. This is different to the density of dust used in the CLASSIC and UKCA dust schemes (2650 kg m^{-3}) and is more representative of, e.g., ammonium sulfate aerosol. Given the Reynold's number with respect to diameter ($R_{e,D}$) determined using Beard's (1976) approach (Section S1 in the Supplement), the critical Stokes number ${S_t}^*$ is then defined as:

$${S_t}^*(D_d) = \frac{1.2 + \frac{1}{12}\ln(1 + R_{e,D})}{1 + \ln(1 + R_{e,D})} \quad \text{(Eq. } S43\text{)}$$

A few variables have been introduced in Eqs S34-S43 and need to be defined. Namely, the characteristic relaxation time of particles (τ, s), the particle Brownian diffusion coefficient (D_{diff}, m^2 s^{-1}), the viscosity of water (μ_w, kg m^{-1} s^{-1}), and the density of water ($\rho_w = 997$ kg m^{-3}). Seinfeld and Pandis (1998) provide formulae for τ and D_{diff} (Eqs S44-S46).

$$\tau(d_p) = \frac{(\rho_p - \rho_a){d_p}^2 C_c(d_p)}{18\mu_a} \quad \text{(Eq. } S44\text{)}$$

$$D_{\text{diff}}(d_p) = \frac{k_B T_a C_c(d_p)}{3\pi\mu_a d_p} \quad \text{(Eq. } S45\text{)}$$

$$C_c(d_p) = 1 + \frac{2\lambda_a}{d_p}\left(1.257 + 0.4\exp\left(-\frac{1.1 d_p}{2\lambda_a}\right)\right) \quad \text{(Eq. } S46\text{)}$$

Dehaoui *et al*. (2015) provide a power law for μ_w in terms of temperature valid from super-cooled water up to the boiling point or $239.15\ \text{K} \le T_a \le 373.15\ \text{K}$ (Eq. S47).

$$\mu_w = 1.3788 \times 10^{-4} \times \left(\frac{T_a}{225.66} - 1\right)^{-1.6438} \quad \text{(Eq. } S47\text{)}$$

S4 Thermophoresis and diffusiophoresis effects

A number of studies have suggested that $E_{\text{slinn}}(D_d, d_p)$ significantly underestimates the collision efficiency, particularly for accumulation sized particles (0.1 μm $< d_p <$ 1 μm), by missing out key processes that affect collision. Various processes have been highlighted as having an impact upon collision, such as thermophoresis, diffusiophoresis, and electric charge. Davenport and Peters (1978), Andronache *et al.* (2006), Wang *et al.* (2010), and various others have provided formulae for these missing effects.

For thermophoresis ($E_{Th}(D_d, d_p)$) and diffusiophoresis ($E_{Df}(D_d)$), the following are applicable:

$$E_{th}(D_d, d_p) = \frac{4\alpha_{th}\left(2 + 0.6\, {R_{e,r}}^{\frac{1}{2}} {P_r}^{\frac{1}{3}}\right)(T_a - T_s)}{U_t(D_d)D_d} \quad \text{(Eq. } S48\text{)}$$

$$E_{df}(D_d) = \frac{4\beta_{dph}\left(2 + 0.6\, {R_{e,r}}^{\frac{1}{2}} {S_{cw}}^{\frac{1}{3}}\right)\left(\frac{p_s^{\circ}}{T_s} - \frac{p_a^{\circ} RH}{T_a}\right)}{U_t(D_d)D_d} \quad \text{(Eq. } S49\text{)}$$

$$\alpha_{th} = \frac{2\left(k_a + {5\lambda_a}/{D_d k_p}\right)k_a C_c(d_p)}{5P_a\left(1 + {6\lambda_a}/{D_d}\right)\left(2k_a + k_p + {10\lambda_a}/{D_d k_p}\right)} \quad \text{(Eq. } S50\text{)}$$

$$P_r = \frac{c_p \mu_a}{k_a} \quad \text{(Eq. } S51\text{)}$$

$$\beta_{dph} = \frac{T_a D_{\text{diffwater}}}{P_a}\left(\frac{M_w}{M_a}\right)^{\frac{1}{2}} \quad \text{(Eq. } S52\text{)}$$

$$S_{cw} = \frac{\mu_a}{\rho_a D_{\text{diffwater}}} \quad \text{(Eq. } S53\text{)}$$

The algorithm is rather involved and requires expressions for the new parameters: the thermal conductivity of air (k_a, J m^{-1} s^{-1} K^{-1}), the thermal conductivity of the particle (k_p, J m^{-1} s^{-1} K^{-1}), the water vapour diffusivity in air ($D_{\text{diffwater}}$, m^2 s^{-1}), the rain droplet surface temperature (T_s, K), and the saturation vapour pressure of water (p_a° and p_s° at temperature T_a and T_s respectively, Pa). In terms of constants, the molar mass of water is $M_w = 0.01802$, the molar mass of dry air is $M_a = 0.02896$ kg mol^{-1}, and the specific heat capacity of air is $c_p = 1003.5$ J kg^{-1} K^{-1}. RH in Eq. S49 is the relative humidity (%), assumed to be 80 % in this study.

From Pruppacher and Klett (2010), we have the following formulae for k_a and $D_{\text{diffwater}}$, where for the latter $T_0 = 273.15$ K and $P_0 = 101{,}325$ Pa.

$$k_a = 418.4 \times (1.04645 + 0.017\, T_a) \times 10^{-5} \qquad (\text{Eq. } S54)$$

$$D_{\text{diffwater}} = 0.211 \times 10^{-4} \times \left(\frac{T_a}{T_0}\right)^{1.94} \left(\frac{P_0}{P_a}\right) \qquad (\text{Eq. } S55)$$

The particulate thermal conductivity (k_p) depends on the aerosol in question. Ladino *et al.* (2011) use a value of 0.419, which is similar to representative values for ammonium sulphate, ammonium nitrate, and soot at 0 °C (0.53). Whereas sea-salt has $k_p = 6.7$ and calcite (mineral dust) is $k_p \approx 3$. For this simple investigation, we assume $k_p = 0.5$ following the logic that this scheme may well be used for all UKCA-mode aerosol in future.

For the surface temperature of rain droplets (T_s), a good assumption is to use the wet-bulb temperature which is always less than the ambient dry-bulb temperature (T_a). For simplicity though, we assume a constant $T_a - T_s$ increment, such that $T_s = T_a - 5$°C as in Davenport and Peters (1978), or $T_s = T_a - 3$ °C as in Wang *et al.* (2010). We choose $T_s = T_a - 3$ °C.

We use the saturation vapour pressure formula from Seinfeld and Pandis (1998), where temperature is in °C and may refer to the air temperature (T_a) or the rain droplet temperature (T_s). The coefficients are $a_0 = 6.107799961$, $a_1 = 4.436518521 \times 10^{-1}$, $a_2 = 1.428945805 \times 10^{-2}$, $a_3 = 2.650648471 \times 10^{-4}$, $a_4 = 3.031240396 \times 10^{-6}$, $a_5 = 2.034080948 \times 10^{-8}$, and $a_6 = 6.136820929 \times 10^{-11}$.

$$p^{\circ} = 100 \times (a_0 + a_1 T + a_2 T^2 + a_3 T^3 + a_4 T^4 + a_5 T^5 + a_6 T^6) \qquad (\text{Eq. } S56)$$

S5 Charged particles

Particles and droplets may attract each other if their charges are of opposite sign, an effect which should be included in the collision efficiency. Andronache *et al.* (2006) use the following relation for the collision efficiency due to charge.

$$E_{es}(D_d, d_p) = \frac{16 K Q_d q_p C_c(d_p)}{3\pi\mu_a U_t(D_d) {D_d}^2 d_p} \qquad (\text{Eq. } S57)$$

$$Q_d = a\alpha {D_d}^2 \qquad (\text{Eq. } S58)$$

$$q_p = a\alpha {d_p}^2 \qquad (\text{Eq. } S59)$$

In Eq. S57, $K = 9 \times 10^9$ N m^2 C^{-2}, while in Eqs S58-S59 $a = 0.83 \times 10^{-6}$. α is an empirically derived parameter that ranges from 0 to 7 C m^{-2} for neutral to highly charged particles respectively. Wang *et al.* (2010) use $\alpha = 2$ based on standard tropospheric conditions.

References

Abel, S. J. and Boutle, I. A.: An improved representation of the raindrop size distribution for single-moment microphysics schemes, Q. J. Roy. Meteorol. Soc., 138, 2151-2162, https://doi.org/10.1002/qj.1949, 2012.

Adler, R. F., Huffman, G. J., Chang, A., Ferraro, R., Xie, P., Janowiak, J., Rudolf, B., Schneider, U., Curtis, S., Bolvin, D., Gruber, A., Susskind, J., and Arkin, P.: The Version 2 Global Precipitation Climatology Project (GPCP) Monthly Precipitation Analysis (1979-Present), J. Hydrometeor, 4,1147-1167, 2003.

Andronache, C., Gr¨nholm, T., Laakso, L., Phillips, V., and Venäläinen, A.: Scavenging of ultrafine particles by rainfall at a boreal site: observations and model estimations, Atmos. Chem. Phys., 6, 4739-4754, doi:10.5194/acp-6-4739-2006, 2006.

Beard, K. V.: Terminal velocity and shape of cloud and precipitation drops aloft, J. Atmos. Sci., 33, 851-864, 1976.

Bohren, C.F., and Albrecht, B.A.: Atmospheric Thermodynamics. New York: Oxford University Press, 402 p., 1998.

Davenport, H. M. and Peters, L. K.: Field studies of atmospheric particulate concentration changes during precipitation, Atmos. Environ., 12, 997-1008, 1978.

Dehaoui, A., Issenmann, B., and Caupin, F.: Viscosity of deeply supercooled water and its coupling to molecular diffusion, P. Natl. Acad. Sci. USA, 112, 12020-12025, doi:10.1073/pnas.1508996112, 2015.

Fredericks, S., and Saylor, J. R.: Parametric investigation of two aerosol scavenging models in the inertial regime, J. Aerosol Sci., 101, 34-42, http://dx.doi.org/10.1016/j.jaerosci.2016.07.011, 2016.

Hill, A. A., Shipway, B. J., and Boutle, I. A.: How sensitive are aerosol-precipitation interactions to the warm rain representation?, J. Adv. Model. Earth Syst., 7, 987–1004, doi:10.1002/2014MS000422., 2015.

Holben, B. N., Eck, T. F., Slutsker, I., Tanre, D., Buis, J. P., Setzer, A., et al.: AERONET – A federated instrument network and data archive for aerosol characterization, Remote Sens. Environ., 66(1), 1-16, 1998.

Huneeus, N., Schulz, M., Balkanski, Y., Griesfeller, J., Prospero, J., Kinne, S., Bauer, S., Boucher, O., Chin, M., Dentener, F., Diehl, T., Easter, R., Fillmore, D., Ghan, S., Ginoux, P., Grini, A., Horowitz, L., Koch, D., Krol, M. C., Landing, W., Liu, X., Mahowald, N., Miller, R., Morcrette, J.-J., Myhre, G., Penner, J., Perlwitz, J., Stier, P., Takemura, T., and Zender, C. S.: Global dust model intercomparison

in AeroCom phase I, Atmos. Chem. Phys., 11, 7781–7816, https://doi.org/10.5194/acp-11-7781-2011, 2011.

Kok, J. F., Adebiyi, A. A., Albani, S., Balkanski, Y., Checa-Garcia, R., Chin, M., Colarco, P. R., Hamilton, D. S., Huang, Y., Ito, A., Klose, M., Leung, D. M., Li, L., Mahowald, N. M., Miller, R. L., Obiso, V., Pérez García-Pando, C., Rocha-Lima, A., Wan, J. S., and Whicker, C. A.: Improved representation of the global dust cycle using observational constraints on dust properties and abundance, Atmos. Chem. Phys., 21, 8127-8167, https://doi.org/10.5194/acp-21-8127-2021, 2021.

Ladino, L., Stetzer, O., Hattendorf, B., Günther, D., Croft, B., and Lohmann, U.: Experimental study of collection efficiencies between sub-micrometer aerosols and cloud droplets, J. Atmos. Sci., 68, 1853-1864, doi:10.1175/JAS-D-11-012.1, 2011.

List, R.: Smithsonian Meteorological Tables, 6th rev. edn., 4th reprint, Washington, DC, 1968.

Marshall, J. S. and Palmer, W.: The distribution of raindrops with size, J. Meteorol., 5, 165–166, 1948.

Prospero, J. M. and Nees, R. T.: Impact of the North African drought and El Niño on mineral dust in the Barbados trade winds, Nature, 320, 735–738, https://doi.org/10.1038/320735a0, 1986.

Pruppacher H. R. and Klett, J. D.: Microphysics of clouds and precipitation; 2nd Edn., Springer, Dordrecht, 954 pp., ISBN 978-0-7923-4211-3, 2010.

Sachidananda, M. and Zrnic, D. S.: Differential propagation phase shift and rainfall rate estimation, Radio Sci., 21, 235–247, 1986.

Seinfeld, J. H. and Pandis, S. N.: Atmospheric Chemistry and Physics, Wiley, New York, USA, 1998.

Sekhon, R. and Srivastava, R.: Doppler observations of drop size distributions in a thunderstorm, J. Atmos. Sci., 28, 983-994, 1971.

Slinn, W. G. N.: Precipitation Scavenging in Atmospheric Science and Power Production, CH. 11, edited by: Randerson, D., Tech. Inf. Cent., Off. of Sci. and Techn. Inf., Dep. of Energy, Washington DC, USA, 466–532, 1984.

Wang, X., Zhang, L., and Moran, M. D.: Uncertainty assessment of current size-resolved parameterizations for below-cloud particle scavenging by rain, Atmos. Chem. Phys., 10, 5685-5705, doi:10.5194/acp-10-5685-2010, 2010.

Wang, X., Zhang, L., and Moran, M. D.: Development of a new semi-empirical parameterization for below-cloud scavenging of size-resolved aerosol particles by both rain and snow, Geosci. Model Dev., 7, 799-819, doi:10.5194/gmd-7-799-2014, 2014.

Symbol	Description	Units	Value	Equation(s)
a	Constant in formulation of E_{es}	-	0.83×10^{-6}	-
B_o	Bond number	-	Derived	S14
c_p	Specific heat capacity of air	J kg^{-1} K^{-1}	1003.5	-
C_c	Cunningham correction factor	-	Derived	S6, S46
d_p	Aerosol diameter	m	Variable	-
D_d	Cloud droplet diameter	m	Variable	-
D_{diff}	Brownian diffusion coefficient	m^2 s^{-1}	Derived	S45
$D_{\text{diffwater}}$	Water vapour diffusivity in air	m^2 s^{-1}	Derived	S55
E	Collision efficiency	-	Derived	S39- S41, S48, S49, S57 Eq. 12 in paper
E_{slinn}	Collision efficiency proposed by Slinn (1984)	-	Derived	S39
E_{br}	Collision efficiency due to Brownian motion	-	Derived	S40
E_{in}	Collision efficiency due to interception	-	Derived	S41
E_{im}	Collision efficiency due to impaction	-	Derived	S42
E_{th}	Collision efficiency due to thermophoresis	-	Derived	S48
E_{df}	Collision efficiency due to diffusiophoresis	-	Derived	S48
E_{es}	Collision efficiency due to electric charge	-	Derived	S57
E_{rc}	Collision efficiency due to rear-capture	-	Derived	Eq. 12 in paper
g	Gravitational acceleration	m s^{-2}	9.8	-
k_B	Boltzmann constant	J K^{-1}	1.3804×10^{-23}	-
k_a	Thermal conductivity of air	J m^{-1} s^{-1} K^{-1}	Derived	S54
k_p	Thermal conductivity of the particle	J m^{-1} s^{-1} K^{-1}	0.5	-
K	Constant in formulation of E_{es}	N m^2 C^{-2}	9×10^9	-
m_a	Molecular mass of dry air	kg	4.78×10^{-26}	-
M_w	Molar mass of water	kg mol^{-1}	0.01802	-

M_a	Molar mass of dry air	kg mol^{-1}	0.02896	-
n	Number density of aerosol particles	m^{-3} m^{-1}	Derived	Lognormal PDF
N	Number density of rain droplets	m^{-3} m^{-1}	Derived	S24
N_0	Intercept of rain droplet distribution	m^{-3} m^{-1}	Derived	S26, S28, S31
N_p	Ratio of Davies to Bond Number	-	Derived	S15
p_a^o	Saturation vapor pressure of water at temperature T_a	Pa	Derived	S56
p_s^o	Saturation vapor pressure of water at temperature T_s	Pa	Derived	S56
P_a	Air pressure	Pa	101,325	-
P_r	Prandtl number	-	Derived	S51
q_p	Mean charge of a particle	C	Derived	S59
Q_d	Mean charge of a rain drop	C	Derived	S58
R	Rainfall rate	mm hr^{-1}	Derived	S23
R_a	Specific gas constant	J kg^{-1} K^{-1}	287.05	-
$R_{e,r}$	Reynolds number according to radius	-	Derived	S22, S34
$R_{e,D}$	Reynolds number according to diameter	-	Derived	S9, S18
RH	Relative Humidity	%	80	-
S	Sutherland constant	K	120	-
S_c	Schmidt number	-	Derived	S35
S_{cw}	Schmidt number for water in air	-	Derived	S53
S_t	Stokes number	-	Derived	S36
S_t^*	Critical Stokes number	-	Derived	S43
T_a	Air temperature	K	293.15	-
T_c	Air temperature in Celsius	^{o}C	20	-
T_s	Droplet surface temperature	K	Derived	$T_a - 3$
T_0	Sutherland constant	K	296.166	-
U_t	Terminal velocity of particle / droplet	m s^{-1}	Derived	S5, S10, S19, S20
α	Parameter in formulation of E_{es}	C m^{-2}	2	-
α_{th}	Variable in formulation of E_{th}	m^2 s^{-1} K^{-1}	Derived	S50
β_{dph}	Variable in formulation of E_{df}	m^2 s^{-1} K Pa^{-1}	Derived	S52
λ	Slope of rain droplet distribution	m^{-1}	Derived	S29

λ_a	Mean free path of air molecules	m	Derived	S4
Λ	Scavenging coefficient	s^{-1}	Derived	S33
μ	Shape of rain droplet distribution	-	0	-
μ_a	Dynamic viscosity of air	kg m^{-1} s^{-1}	Derived	S3
μ_w	Viscosity of water	kg m^{-1} s^{-1}	Derived	S47
μ_0	Sutherland constant	kg m^{-1} s^{-1}	1.83×10^{-5}	-
v_a	Mean speed of air molecules	m s^{-1}	Derived	S2
ρ_a	Air density	kg m^{-3}	Derived	S1
ρ_p	Aerosol density	kg m^{-3}	1500	-
ρ_w	Density of water	kg m^{-3}	997	-
$\sigma_{w,a}$	Surface tension of water	N m^{-1}	Derived	S11, S12, S13
τ	Relaxation time of particles	s	Derived	S44
ϕ	Diameter ratio	-	Derived	S37
ω	Ratio of water to air viscosity	-	Derived	S38

Table S1. All variables and their values used in BCS models (Sections S1-S5)

Constants in the Wang *et al.* (2014) Λ_{rain} parameterization							
	$i = 0$	$i = 1$	$i = 2$	$i = 3$	$i = 4$	$i = 5$	$i = 6$
a_i	-6.2609 $\times 10^{0}$	6.8200 $\times 10^{-1}$	8.6760 $\times 10^{-1}$	1.2820 $\times 10^{-1}$			
b_i	-1.4707 $\times 10^{1}$	5.1043 $\times 10^{1}$	-9.7306 $\times 10^{1}$	9.7946 $\times 10^{1}$	-5.3923 $\times 10^{1}$	1.5311 $\times 10^{1}$	-1.7510 $\times 10^{0}$
c_i	7.2300 $\times 10^{-1}$	3.0300 $\times 10^{-2}$					
d_i	-6.4920 $\times 10^{-1}$	9.3483 $\times 10^{0}$	-2.1929 $\times 10^{1}$	2.5317 $\times 10^{1}$	-1.5395 $\times 10^{1}$	4.7242 $\times 10^{0}$	-5.7660 $\times 10^{-1}$

Table S2. Constants in the Wang *et al.* (2014) Λ_{rain} parameterization

Station	Latitude	Longitude	440 nm aerosol optical depth (AOD)			
			Dec-Feb	Mar-May	Jun-Aug	Sep-Nov
Agoufou Mali	15.3454N	1.47912W	0.3232	0.6905	0.6840	0.4195
Ouagadougou Burkina Faso	12.2N	1.4W	0.4650	0.7370	0.4737	0.4576
Cape Verde	16.7325N	22.9355W	0.2732	0.2995	0.5246	0.3834
Banizoumbou Niger	13.5412N	2.66475E	0.3789	0.7418	0.5549	0.4196
Dakar Senegal	14.3942N	16.9586W	0.3354	0.5098	0.6018	0.4061
Cinzana Mali	13.2784N	5.93387W	0.3547	0.6924	0.5338	0.3504
Tamanrasset Algeria	22.79N	5.53E	0.0708	0.2617	0.4600	0.2269
Zinder airport Niger	13.7767N	8.99023E	0.4571	0.6803	0.5437	0.4350

Table S3. AERONET 440 nm seasonal aerosol optical depth in 8 dusty regions (Holben *et al*., 1998)

Station	Latitude	Longitude	Near surface dust concentration (μg m^{-3})			
			Dec-Feb	Mar-May	Jun-Aug	Sep-Nov
Cape Grim Tasmania	40.68S	144.68E	2.4780	1.7105	0.6190	1.2105
Marsh King George Island	62.18S	58.3W	0.9245	0.7345	0.2745	0.3245
Mawson Antarctica	67.6S	62.5E	0.2210	0.0325	0.0340	0.1295
Palmer Station Antarctica	64.77S	64.05W	0.1050	0.4805	0.6995	0.2085
Funafuti Tuvalu	8.5S	179.2W	0.0865	0.0795	0.1845	0.3785
Menen Point Nauru	0.53S	166.95E	0.0705	0.2715	0.0585	0.0725
Norfolk Island	29.08S	167.98E	0.7620	0.5960	0.1075	2.3480
American Samoa	14.25S	170.58W	0.1880	0.1610	0.1290	0.0770
Midway Island	28.22N	177.35W	0.2475	1.7720	0.3055	0.3720
Oahu Hawaii	21.33N	157.7W	0.5230	1.3455	0.3650	0.2495
Cheju – Korea	33.52N	126.48E	8.4510	25.4015	6.0175	11.5470
Fanning Island	3.92N	159.33W	0.0380	0.2675	0.0405	0.0385
Enewetak Atoll	11.33N	162.33E	0.1375	0.4390	0.1800	0.0885
Ragged Point Barbados	13.17N	59.43W	4.9480	15.1195	30.5450	18.2140
Bermuda West and East	32.27N	64.87W	0.3425	1.2325	7.1990	3.0560
Mace Head Ireland	53.32N	9.85W	0.9940	1.2820	1.0205	0.7625
University of Miami – Florida	25.75N	80.25W	1.2365	1.7260	14.2730	2.6590
Izana Tenerife (alt=2360 m)	28.3N	16.5W	8.3015	39.8525	33.9970	31.1735

Table S4. Seasonal near surface dust concentrations from the University of Miami Oceanic Aerosols Network (U-MIAMI) (Prospero and Nees, 1986)

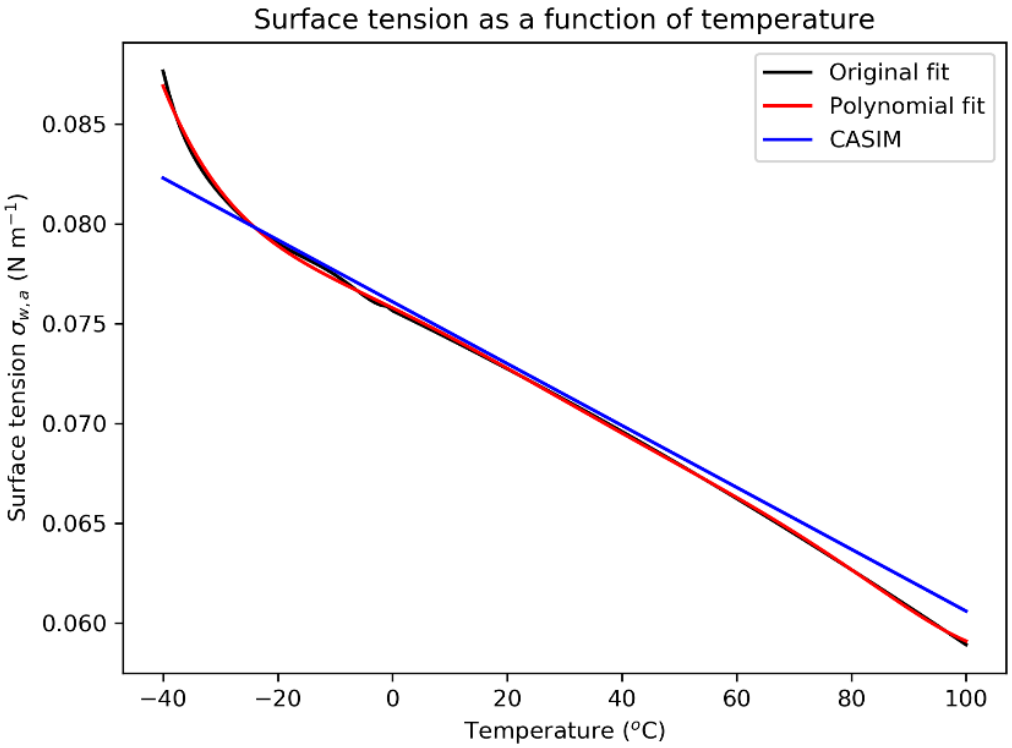

Figure S1. Surface tension $\sigma_{w,a}$ as a function of temperature T_c. Cloud AeroSol Interaction Microphysics (CASIM) is a new cloud microphysics model at the Met Office (Hill *et al.*, 2015) and is shown for reference

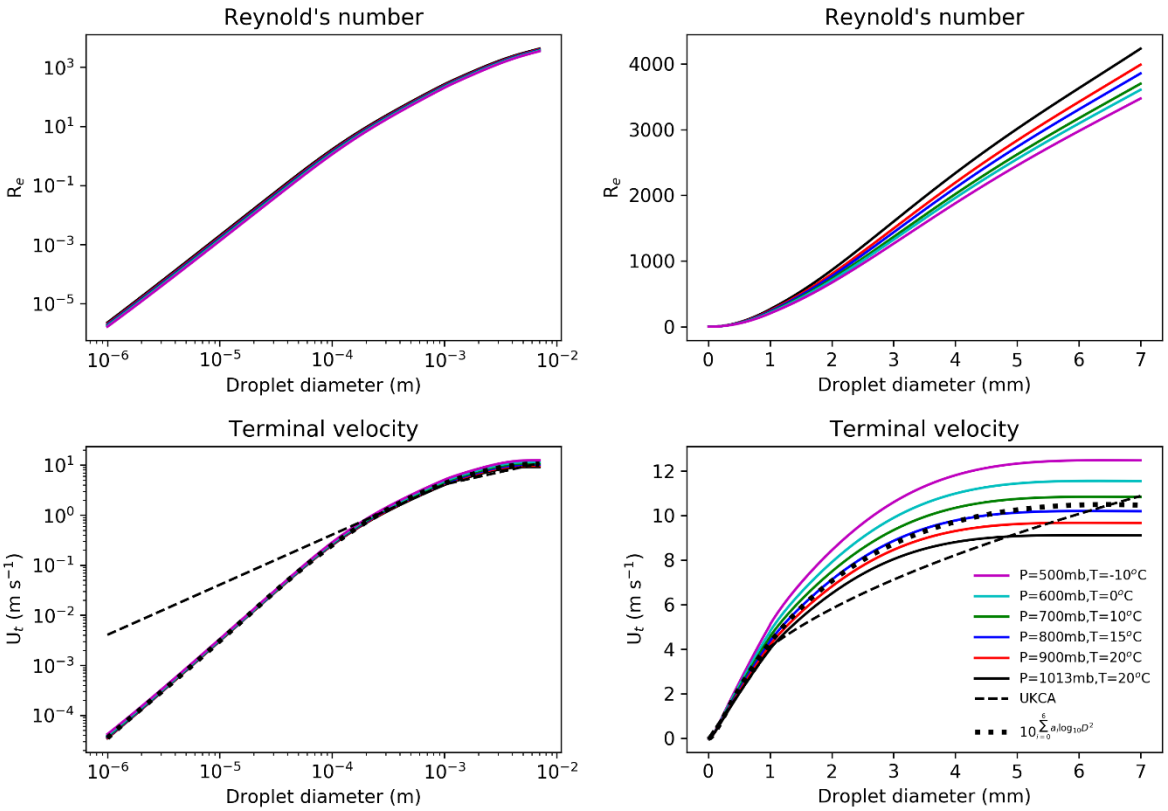

Figure S2. Reynold's number ($R_{e,D}$) and terminal velocity (U_t) as a function of droplet diameter (D_d) for various standard atmospheric conditions using the Beard (1976) scheme alongside U_t as parameterised in UKCA and the parameterisation given in Eq. S21.

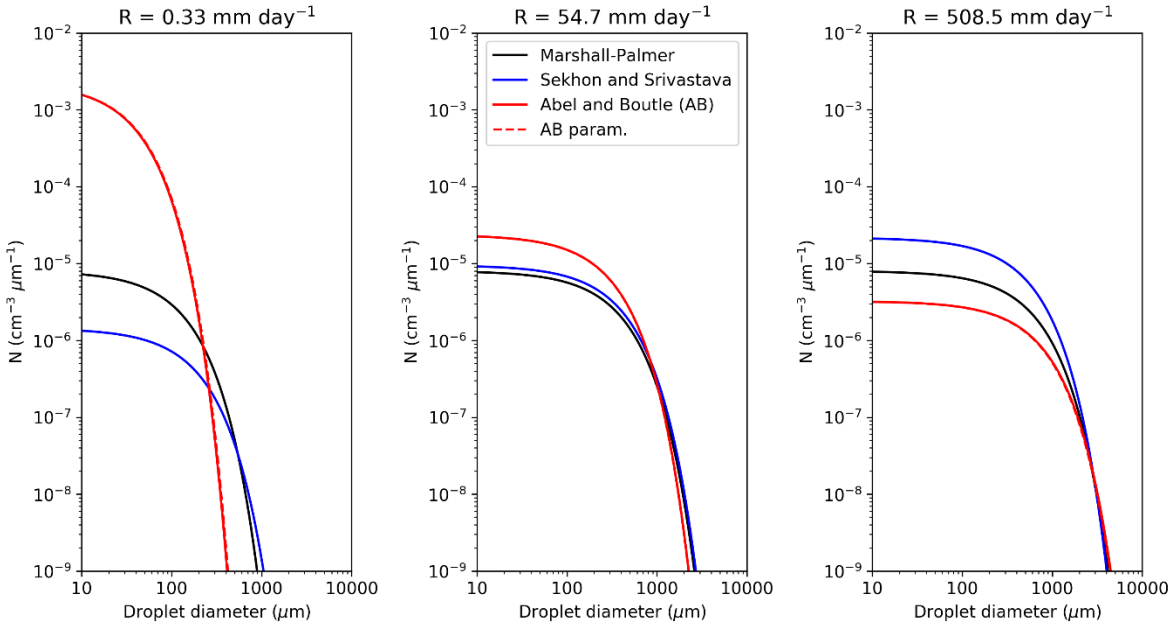

Figure S3. The rain droplet number distribution for various rainfall rates (*R*) and 3 different parameterisations assuming an exponential distribution

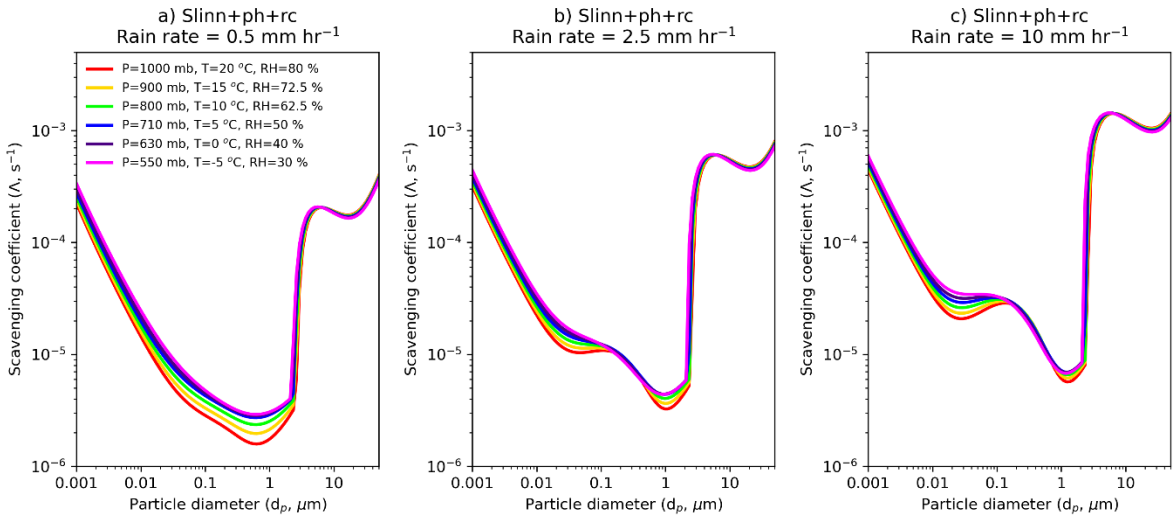

Figure S4. BCS scavenging coefficient for the *Slinn+ph+rc* model as a function of aerosol diameter for various atmospheric profiles representative of 1 km altitude increments from the surface to 5 km

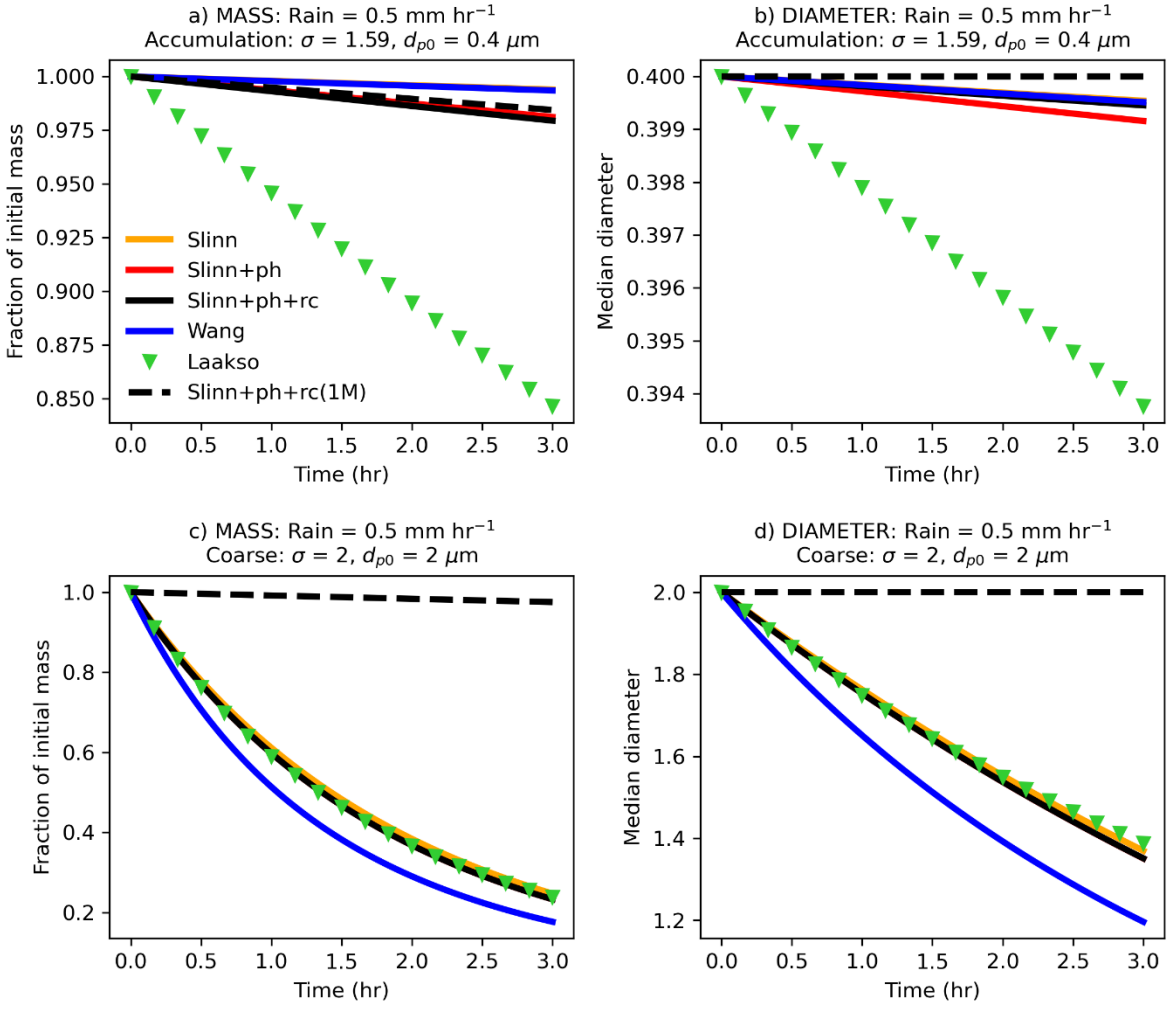

Figure S5a. Time evolution of the (a,c) mass concentration and (b,d) median diameter of (a-b) an accumulation-like mode and (c-d) a coarse-like mode with a constant rain rate of 0.5 mm hr^{-1} for 6 BCS schemes. Results from offline box model simulations

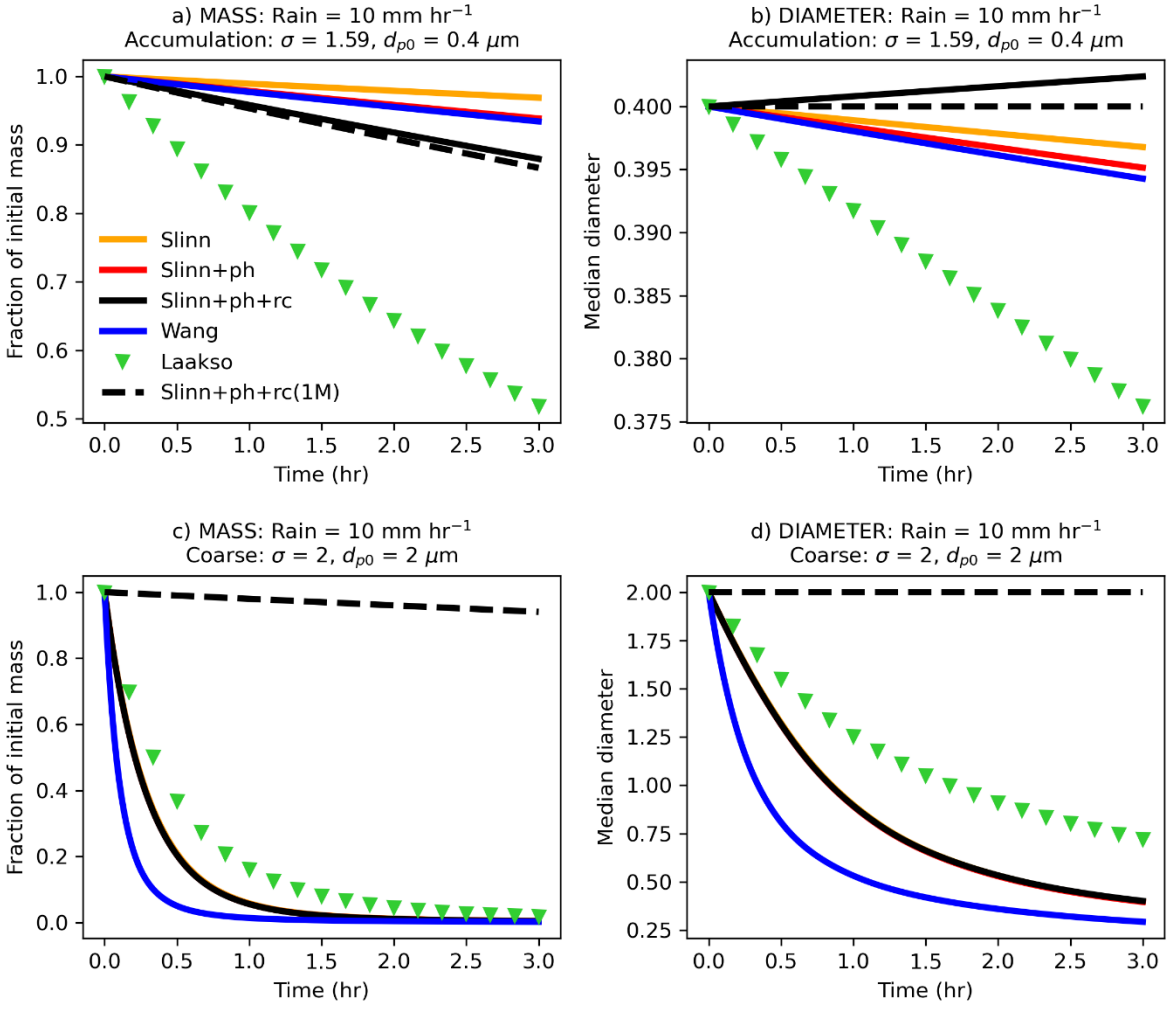

Figure S5b. Time evolution of the (a,c) mass concentration and (b,d) median diameter of (a-b) an accumulation-like mode and (c-d) a coarse-like mode with a constant rain rate of 10 mm hr^{-1} for 6 BCS schemes. Results from offline box model simulations

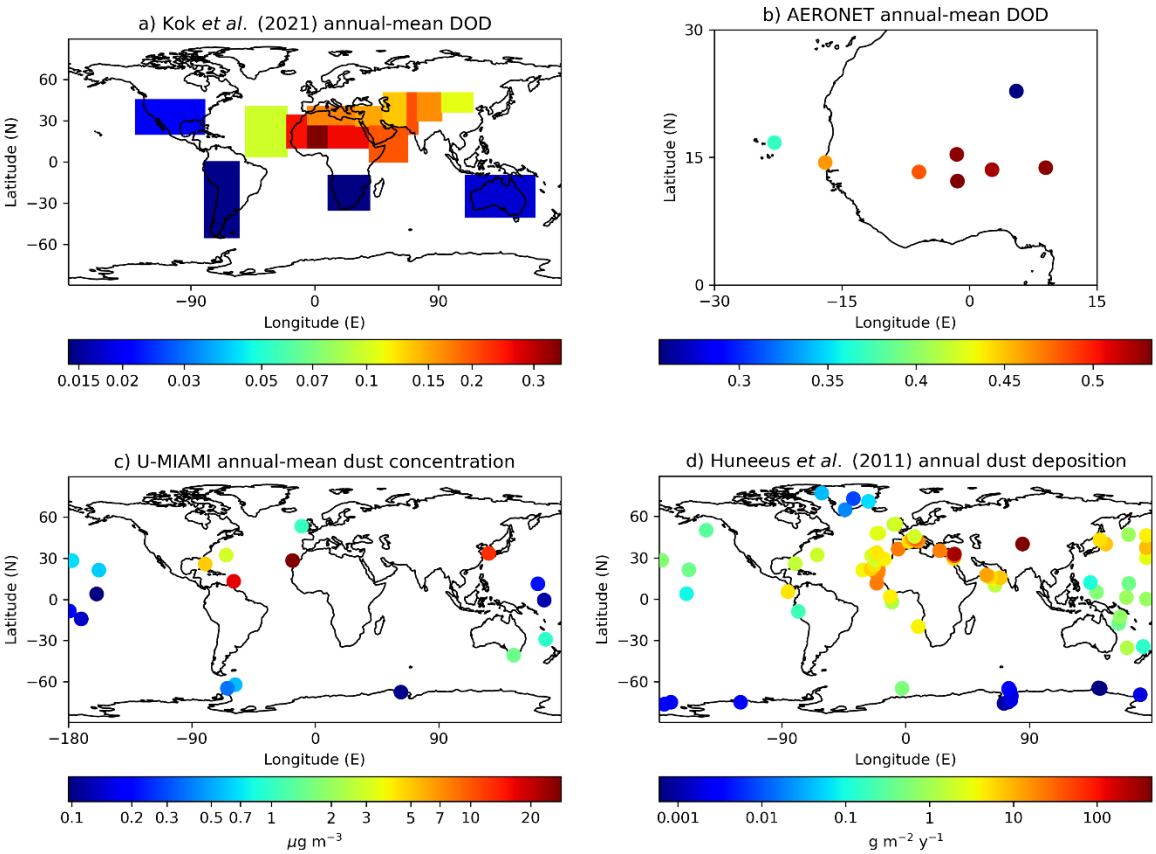

Figure S6. Annual-mean values by area or station from 4 datasets used to assess simulated dust in the UM-GA8.0 simulations: (a) 550 nm dust optical depth (DOD) from Kok *et al*. (2021), (b) 440 nm DOD from AERONET measurements (Table S3), (c) near surface dust concentration from the U-MIAMI dataset (Table S4, Prospero and Nees, 1986), and (d) dust deposition rates from Huneeus *et al.* (2011)

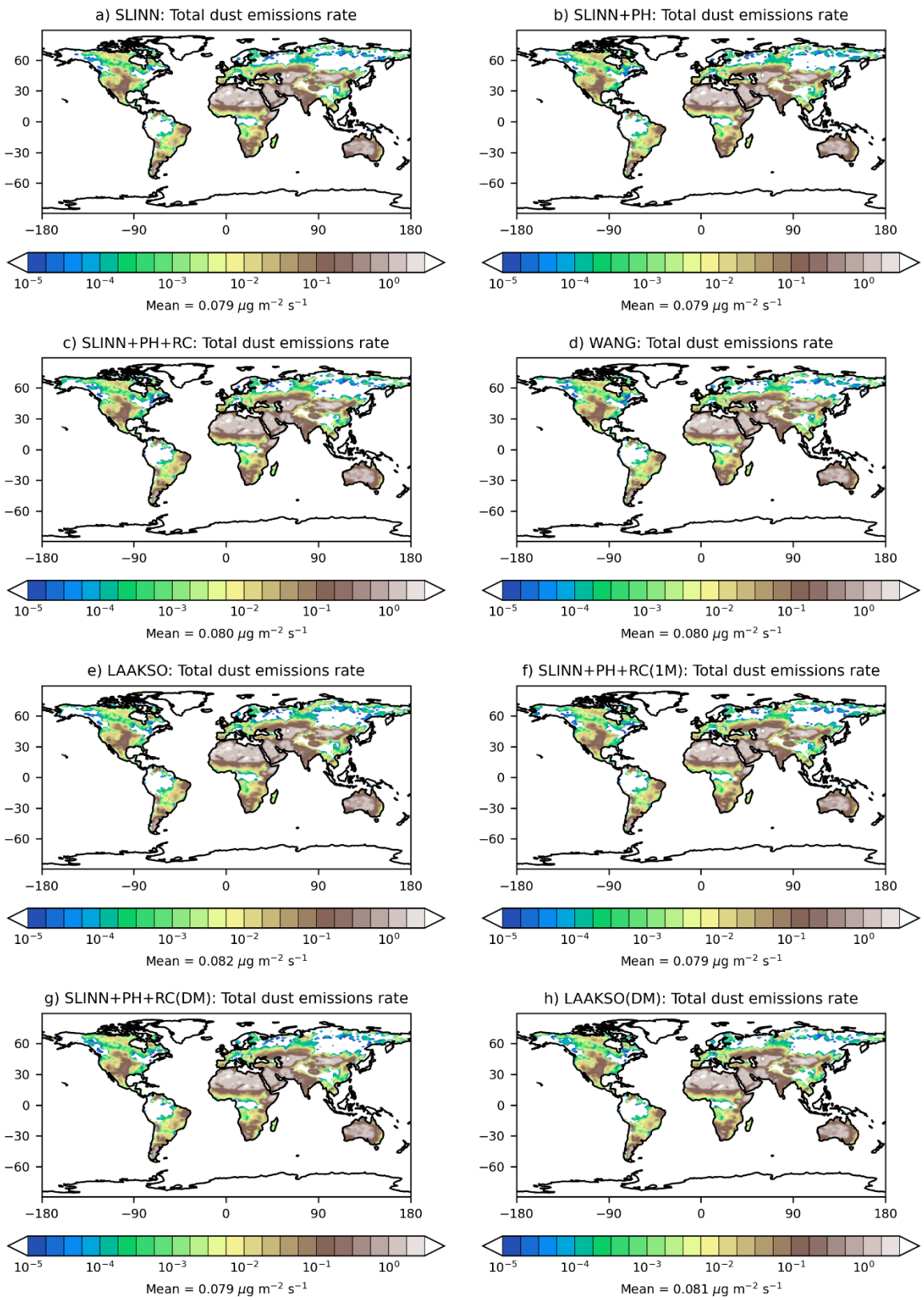

Figure S7. Annual-mean total dust emissions rate in all of the UM-GA8.0 simulations performed for this study

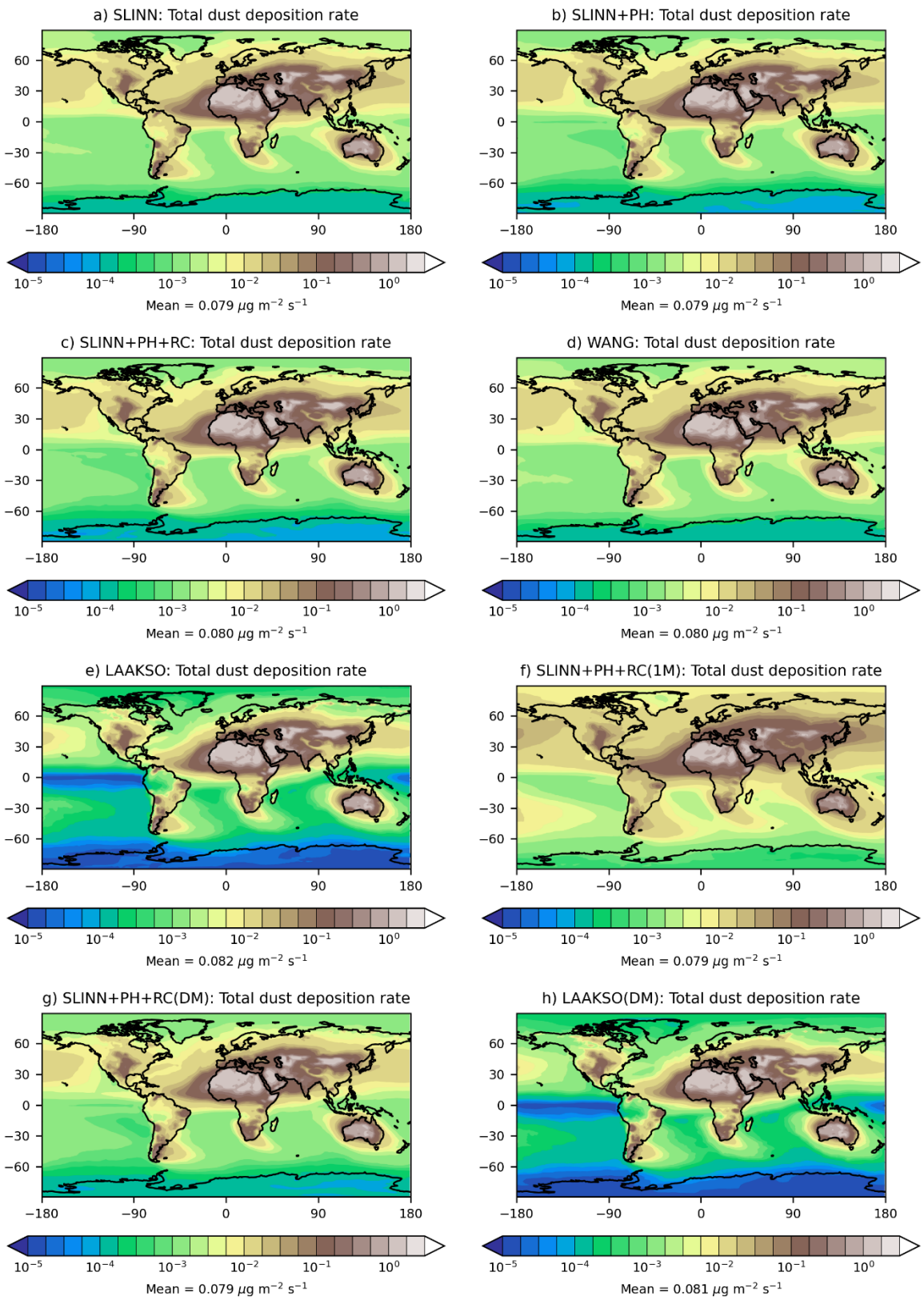

Figure S8. Annual-mean total dust deposition rate in all of the UM-GA8.0 simulations performed for this study

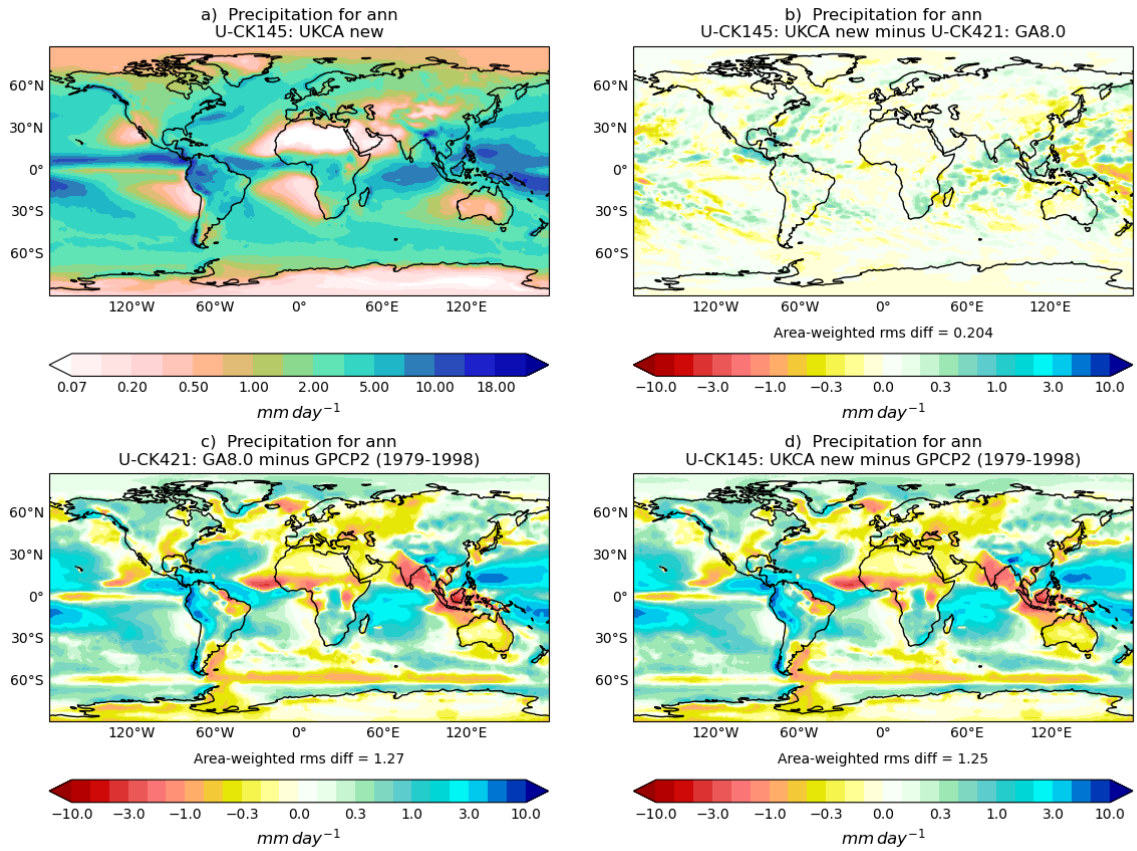

Figure S9. Annual-mean precipitation anomalies with respect to observations from the Global Precipitation Climatology Project (GPCP2) (Adler *et al.*, 2003). (a) Annual mean precipitation in the SLINN+PH+RC simulation (i.e., u-ck145, (b) the difference between precipitation in SLINN+PH+RC and the default UM-GA8.0 model (i.e., u-ck421) which employs CLASSIC dust, (c) the difference between precipitation in default UM-GA8.0 and GPCP2, and (d) the difference between precipitation in SLINN+PH+RC and GPCP2

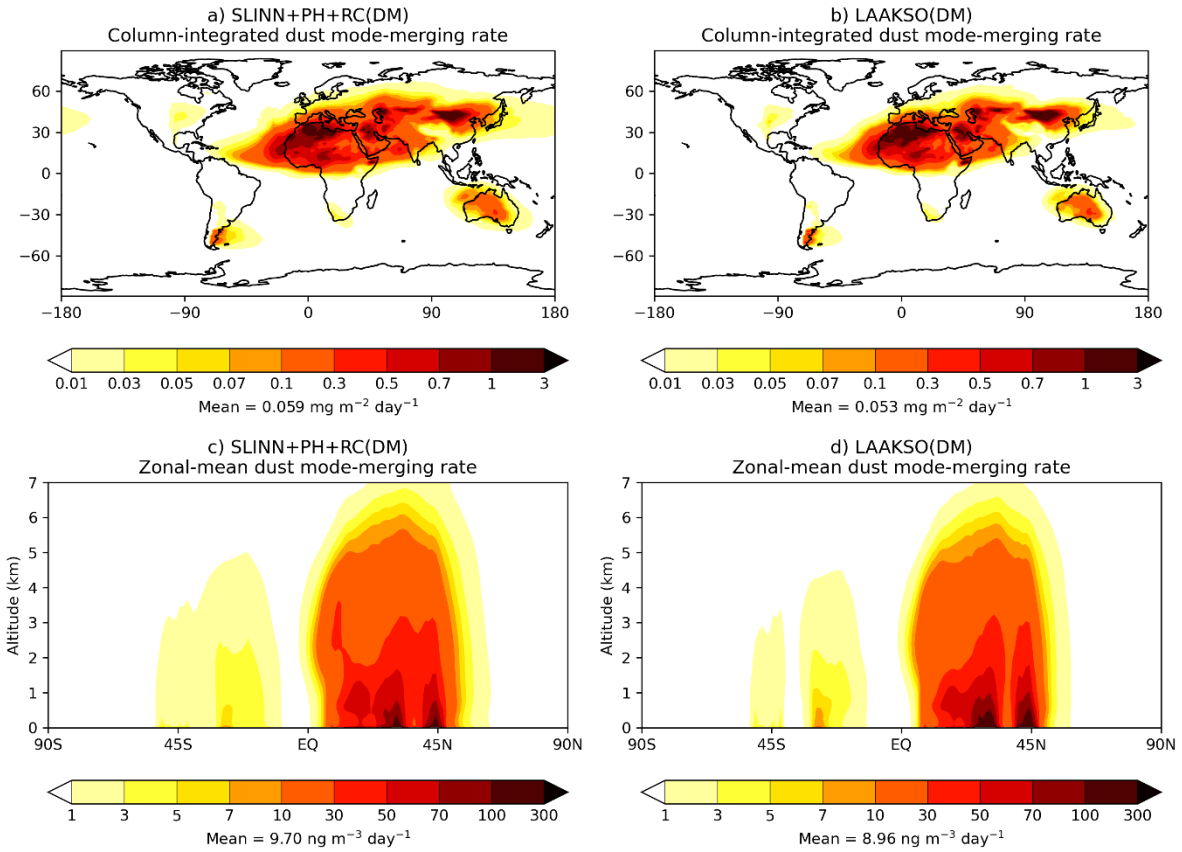

Figure S10. Annual-mean dust mode merging rate (coarse mode → accumulation mode): (a) integrated vertically in SLINN+PH+RC(DM), (b) integrated vertically in LAAKSO(DM), (c) zonally averaged in SLINN+PH+RC(DM), and (d) zonally averaged in LAAKSO(DM)

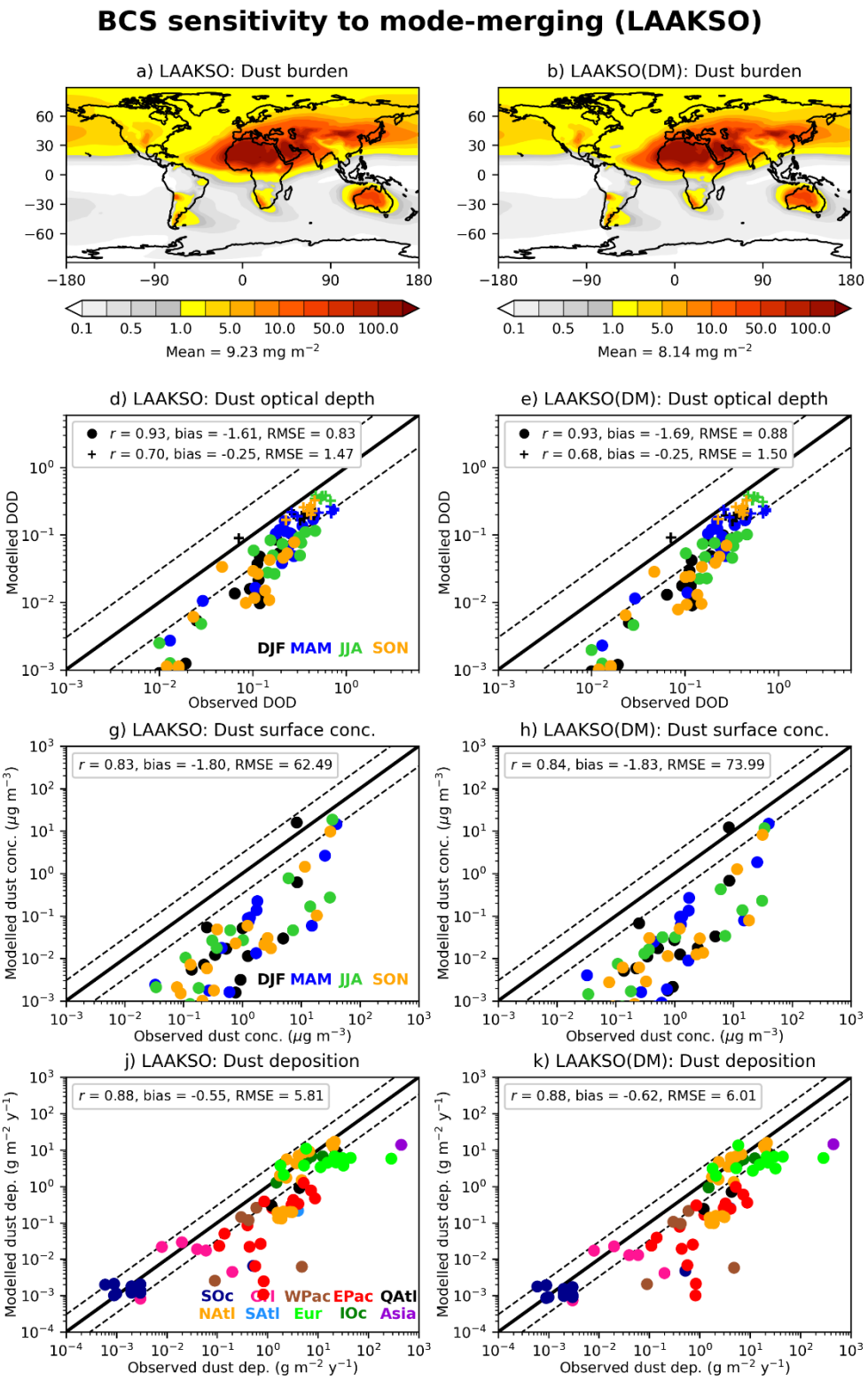

Figure S11. Global dust metrics in the LAAKSO and LAAKSO(DM) simulations, used to answer KQ4 – impact of representing downward mode-merging. (a-c) annual-mean total dust burden, (d-f) seasonal and regional dust optical depths (DOD) against 440n nm AERONET observations (+) and 550nm DOD from Kok *et al.* (2021), (g-i) seasonal and regional near surface dust concentrations against U-MIAMI observations (Prospero and Nees, 1986), (j-l) annual-mean regional dust deposition rates against observations from Huneeus *et al.* (2011)

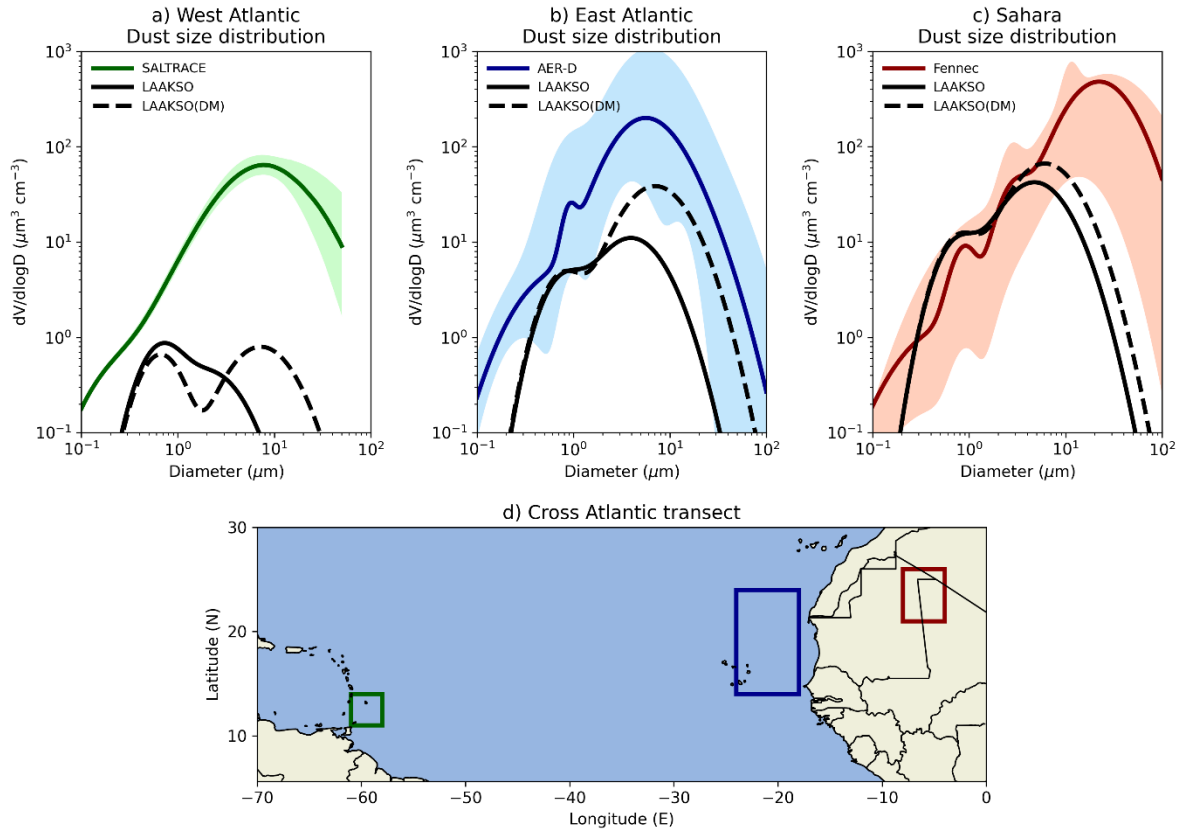

Figure S12. Dust volume size distributions in a cross Atlantic transect in the LAAKSO and LAAKSO(DM) simulations for (a) June conditions in the region (58-61 ºW, 11-14 ºN) and 2-2.4 km compared to SALTRACE measurements, (b) August conditions in the region (18-24 ºW, 14-24 ºN) and 2-3 km altitude compared to AER-D measurements, and (c) June conditions in the region (4-8 ºW, 21-26 ºN) and 0.1-1.2 km altitude compared to Fennec 2011 measurements. (d) shows the horizontal boundaries of the averaging regions in the Equatorial Atlantic

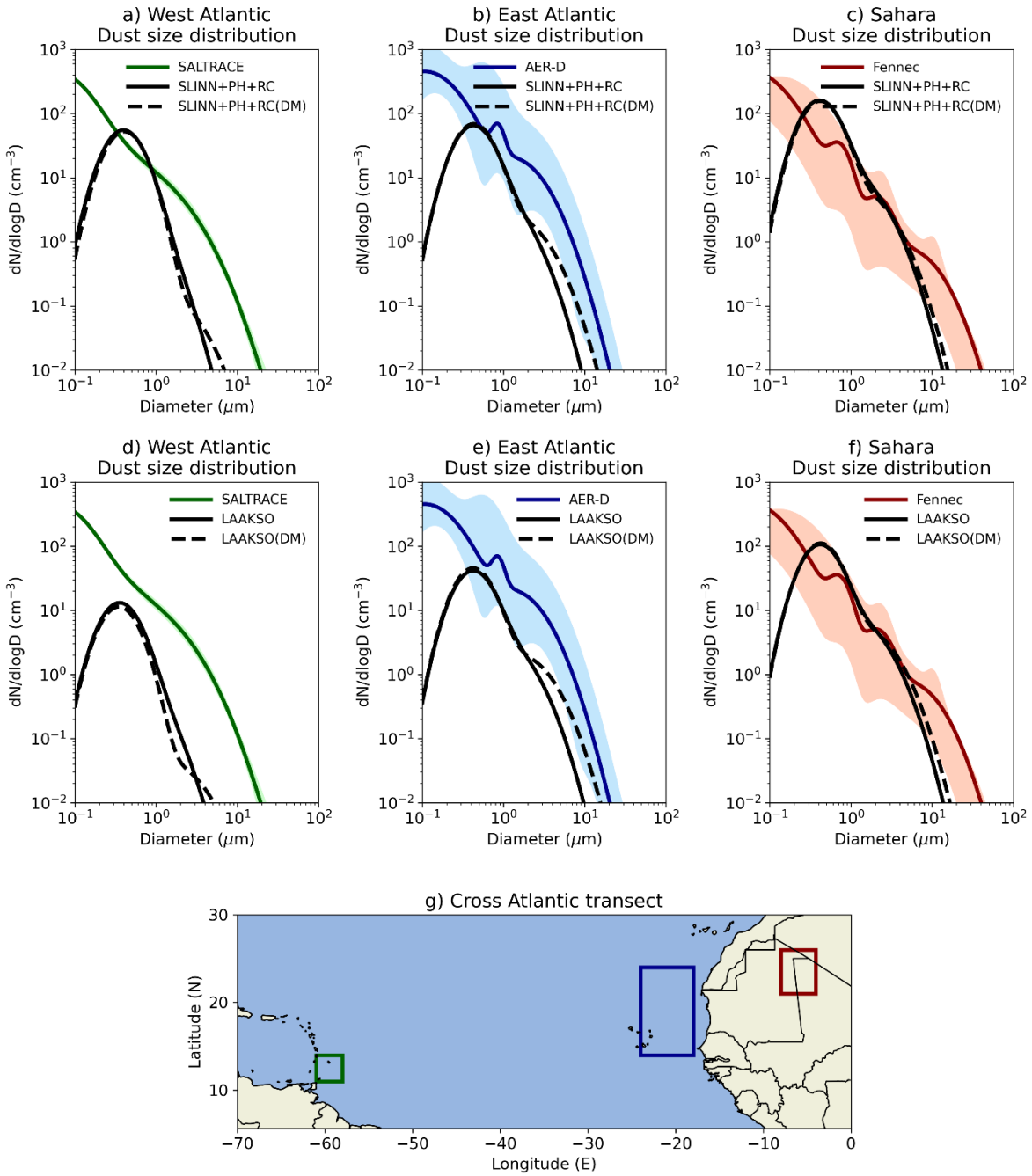

Figure S13. Dust number size distributions in a cross Atlantic transect in the SLINN+PH+RC and SLINN+PH+RC(DM) simulations (a-c) and LAAKSO and LAAKSO(DM) simulations (d-f) for: (a,d) June conditions in the region (58-61 ºW, 11-14 ºN) and 2-2.4 km compared to SALTRACE measurements, (b,e) August conditions in the region (18-24 ºW, 14-24 ºN) and 2-3 km altitude compared to AER-D measurements, and (c,f) June conditions in the region (4-8 ºW, 21-26 ºN) and 0.1-1.2 km altitude compared to Fennec 2011 measurements. (g) shows the horizontal boundaries of the averaging regions in the Equatorial Atlantic